Journal of Sound and Vibration (1999) **226**(1), 125–147
Article No. jsvi.1999.2289, available online at http://www.idealibrary.com on IDEAL®

FREE VIBRATION OF A ROTATING TAPERED COMPOSITE TIMOSHENKO SHAFT

W. KIM

Department of Mechanical Engineering and Applied Mechanics, University of Michigan, Ann Arbor, MI 48109, *U.S.A.*

A. ARGENTO

Department of Mechanical Engineering, University of Michigan-Dearborn, Dearborn, MI 48128, *U.S.A.*

AND

R. A. SCOTT

Department of Mechanical Engineering and Applied Mechanics, University of Michigan, Ann Arbor, MI 48109, *U.S.A.*

(*Received* 4 *December* 1998, *and in final form* 22 *March* 1999)

A mechanical model is developed of a tapered, filament-wound composite, Timoshenko shaft which is rotating at constant speed about its axis. The model represents an extended length cutting tool intended for use in high-speed operations. The effects of shaft tapering and the use of composite materials on the structure's free response are studied. The spatial solutions to the equations of motion are carried out using the general Galerkin method. It is found that by tapering, bending natural frequencies and stiffness can be significantly increased over those of uniform shafts having the same volume and made of the same material. The potential for designing a taper function to meet a particular cutting need is also discussed. Various composite laminate cases are treated and it is found that improvements of performance are possible over equivalent steel shafts.

1. INTRODUCTION

Vibration of the cutting tool in boring and milling operations can make it very difficult to meet surface finish and dimensional accuracy requirements of the workpiece, can generate excessive amounts of noise and can lead to premature tool failure. The vibration is mainly induced and maintained by forces generated by the cutting process itself and can be a problem of dynamic instability. So, the influence of the cutting tool structure on the dynamic response in the cutting process is of great importance.

Increasing the static bending stiffness of the cutting tool can be desirable because insufficient static bending stiffness is responsible for poor machining accuracy [1, 2]. Also, higher natural frequencies of the cutting tool are beneficial [3] when one is operating at cutting frequencies less than the fundamental frequency. Thus,

0022-460X/99/360125 + 23 $30.00/0

increases in the structural static bending stiffness and first bending natural frequency can have beneficial effects.

One of the possible methods of reducing vibration is structural redesign. By tapering the rotating shaft of the machine tool, the static bending stiffness and the first bending natural frequency can be higher than those of a non-tapered cylindrical shaft which has the same volume. Also, different materials can be used. Fiber-reinforced composite materials have recently received great interest in the machine tool industry [4, 5] because of low weight, high stiffness-to-weight ratio and damping characteristics.

The free and forced vibration of rotating, uniform, isotropic shafts has been widely studied in detail in the field of rotor dynamics for various shaft models and boundary conditions (see, for example, reference [6]). Vibration of rotating, tapered, isotropic material shafts has also been studied. See, for example, the development of finite element methods by Rouch and Kao [7] and Genta and Gugliotta [8]. The work of Maday [9] on the design of minimum weight rotating shafts, using a minimum principle, should also be noted. Fewer works are available for rotating composite material shafts. Uniform cases have recently been treated in references [10–12]. In these studies, coupling effects due to anisotropic properties of composite materials were investigated. Regarding non-uniform rotating composite structures, one available work is that of Bauchau [13] on hollow shafts in which optimization of the wall-thickness tapering is treated using Rayleigh quotient ideas. In the present work, a mechanical model is developed of a tapered, filament-wound composite, Timoshenko shaft which rotates at constant speed about its axis. The spatial solutions are obtained using the general Galerkin method. Numerical results are presented for steel and high modulus graphite/epoxy shafts. The model includes bending, torsional and extensional vibrations.

2. DERIVATION OF THE EQUATIONS OF MOTION

The use of layered composite materials and tapering leads to considerable complications in the derivation of the equations of motion. Here, the main modelling issues are highlighted and specific lengthy manipulations are omitted in the interest of space.

Figure 1 shows a portion of a tapered shaft rotating at a constant angular speed Ω about its axis, z (in the undeformed state). The shaft is taken to be transmitting an axial force P, a torque T, shear forces V_x and V_y and bending moments M_x and M_y. These stress resultants can be determined once the stress distribution is known. For example

$$M_x = \int_A y\sigma_z \, \mathrm{d}A. \tag{1}$$

Figure 2 shows a single lamina (layer) wrapped around a tapered cylinder of taper angle α (which could be a function of z). The axes $1'$ and $3'$ are along and perpendicular to the cylinder surface, respectively. Material principal directions are denoted by 1, 2, 3, the fiber angle β being the angle between the 1 and $1'$ axes.

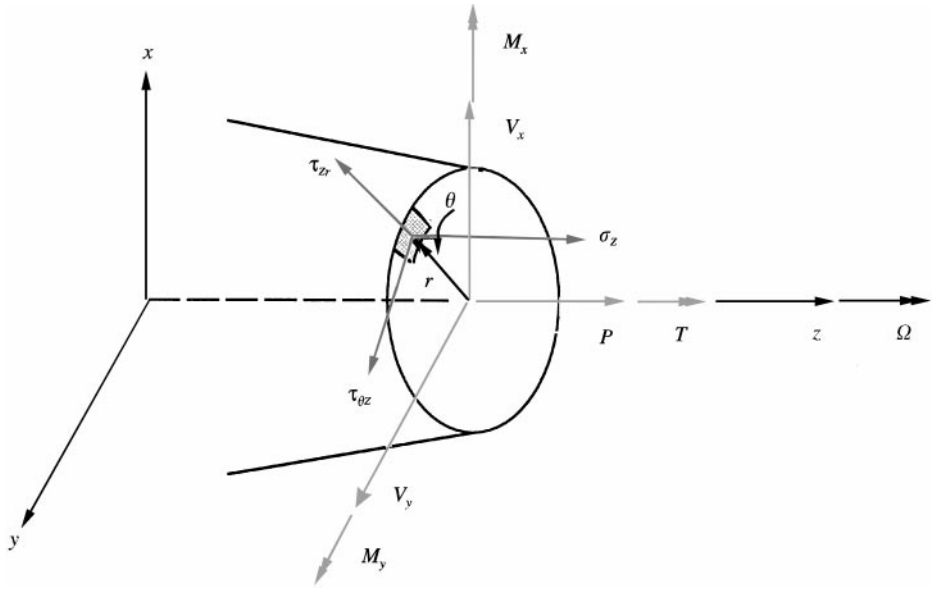

Figure 1. Portion of a tapered shaft rotating at a constant speed Ω about the z-axis.

The stress–strain relations with respect to the cylindrical co-ordinate system r, θ, z are required and are found by a sequence of transformations. For the material co-ordinate system one has (superscript T denotes transpose)

$$[\sigma_{11}\ \sigma_{22}\ \sigma_{33}\ \tau_{23}\ \tau_{31}\ \tau_{12}]^{\mathrm{T}} = [C_{ij}]\,[\varepsilon_{11}\ \varepsilon_{22}\ \varepsilon_{33}\ \gamma_{23}\ \gamma_{31}\ \gamma_{12}]^{\mathrm{T}}, \tag{2}$$

where the C_{ij} are known functions of the layer material parameters (see Jones [14]). The 1, 2, 3 axes are related to the 1′, 2′, 3′ axes by a rotation matrix $[T_\beta]$ and using this the primed and unprimed stresses and strains can be related. Then the primed components are transformed to r, θ, z components by means of a rotation matrix $[T_\alpha]$. The end product is a result of the form

$$[\sigma_r\ \sigma_\theta\ \sigma_z\ \tau_{\theta z}\ \tau_{zr}\ \tau_{r\theta}]^{\mathrm{T}} = [K_{ij}]\,[\varepsilon_r\ \varepsilon_\theta\ \varepsilon_z\ \gamma_{\theta z}\ \gamma_{zr}\ \gamma_{r\theta}]^{\mathrm{T}}, \tag{3}$$

where the K_{ij} are complicated functions of α, β and layer material properties and are given in Appendix A.

A goal of the work is the development of a beam type theory for the problem at hand, rather than the pursuit of elasticity solutions (which are unlikely to exist) or shell theories. In this spirit, some approximations have to be made. Since $\tau_{2'3'}$ is zero on the lateral surface and the shaft is taken to be slender, it is assumed that $\tau_{2'3'} \equiv 0$. Using transformation equations, this condition gives

$$\tau_{r\theta} = -\,\tau_{\theta z} \tan \alpha. \tag{4}$$

In beam theories, σ_r and σ_θ are typically set to zero. In this work, it is expected that the high rotational speeds may produce significant values of these stress

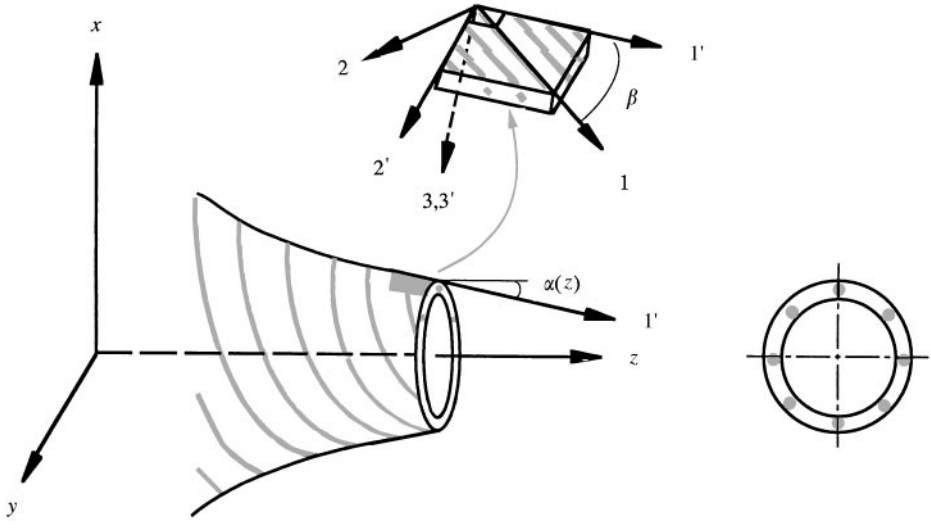

Figure 2. Single lamina of a tapered, filament-wound composite shaft.

components and so they are retained in the formulation. For the moment, their specific forms are left unspecified but they are assumed to be axisymmetric. Substituting the fourth and sixth equations of equations (3) into equation (4) gives a relationship between the six strains. Using this relationship and the first and second equations of equations (3), ε_r, ε_θ and $\gamma_{r\theta}$ may be expressed in terms of ε_z, $\gamma_{\theta z}$, γ_{zr}, σ_r and σ_θ. Using the resulting expressions, the third, fourth and fifth equations of equations (3) lead to expressions of the form (a superscript k has been added to denote that the expressions are for the kth layer)

$$[\sigma_z^{(k)}\ \tau_{\theta z}^{(k)}\ \tau_{zr}^{(k)}]^{\mathrm{T}} = [\bar{K}_{ij}^{(k)}]\,[\varepsilon_z^{(k)}\ \gamma_{\theta z}^{(k)}\ \gamma_{zr}^{(k)}]^{\mathrm{T}} + [\bar{C}_{ij}^{(k)}]\,[\sigma_r^{(k)}\ \sigma_\theta^{(k)}]^{\mathrm{T}}, \tag{5}$$

where $[\bar{K}_{ij}^{(k)}]$ and $[\bar{C}_{ij}^{(k)}]$ are known matrices (details are not given).

A Timoshenko model is adopted for the transverse vibrations. It is assumed that the entire cross-section perpendicular to the z-axis remains a plane after deformation. Figure 3 shows a projection of a deformed element onto the xz-plane (a prime denotes a derivative with respect to z). From this figure and a similar one for the yz-plane, it follows that

$$\varepsilon_z = u_z' - \psi_x' x + \psi_y' y = u_z' - \psi_x' r\cos\theta + \psi_y' r\sin\theta, \tag{6}$$

$$\gamma_{zr} = \gamma_{zx}\cos\theta + \gamma_{zy}\sin\theta = (u_x' - \psi_x)\cos\theta + (u_y' + \psi_y)\sin\theta, \tag{7}$$

$$\gamma_{\theta z} = -\gamma_{zx}\sin\theta + \gamma_{zy}\cos\theta + r\phi' = -(u_x' - \psi_x)\sin\theta + (u_y' + \psi_y)\cos\theta + r\phi'. \tag{8}$$

Here u_x, u_y, u_z are displacements of the neutral axis in the x, y, z directions, respectively, ψ_x and ψ_y denote rotation angles about the y- and x-axis, respectively, and ϕ is the angle of twist. Note that it has been assumed that warping of the cross-section, if it exists, is negligibly small.

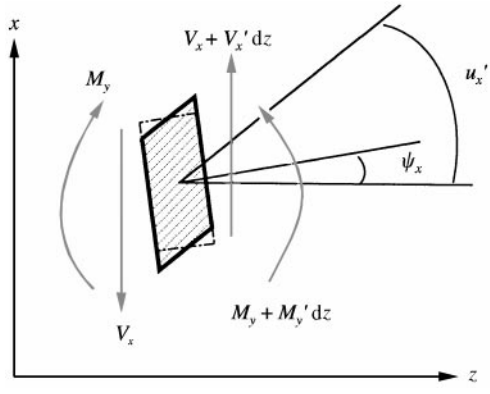

Figure 3. Projection of a deformed element onto the xz-plane.

In Timoshenko beam theory, so-called shear coefficients are frequently introduced as "adjustment factors". The choice of their values is problematical, particularly for problems such as the one at hand involving composite materials and tapering. Here shear coefficients are incorporated into the theory as follows. Equations (7) and (8) may be written as

$$\gamma_{zr} = \gamma_{zrB}, \qquad \gamma_{\theta z} = \gamma_{\theta zB} + \gamma_{\theta zT}, \tag{9, 10}$$

where

$$\gamma_{\theta zT} = r\phi'. \tag{11}$$

The subscripts B and T refer to bending and torsional contributions, respectively. With this notation, equation (5) may be written as

$$[\sigma_z^{(k)}\ \tau_{\theta z}^{(k)}\ \tau_{zr}^{(k)}]^{\mathrm{T}} = [\bar{K}_{ij}^{(k)}]_B\,[\varepsilon_z^{(k)}\ \gamma_{\theta zB}^{(k)}\ \gamma_{zrB}^{(k)}]^{\mathrm{T}} + [\bar{K}_{ij}^{(k)}]_T\,[0\ \gamma_{\theta zT}^{(k)}\ 0]^{\mathrm{T}} + [\bar{C}_{ij}^{(k)}]\,[\sigma_r^{(k)}\ \sigma_\theta^{(k)}]^{\mathrm{T}}, \tag{12}$$

where

$$[\bar{K}_{ij}^{(k)}]_B = \begin{bmatrix} \bar{K}_{11}^{(k)} & \kappa\bar{K}_{12}^{(k)} & \kappa\bar{K}_{13}^{(k)} \\ \bar{K}_{21}^{(k)} & \kappa\bar{K}_{22}^{(k)} & \kappa\bar{K}_{23}^{(k)} \\ \bar{K}_{31}^{(k)} & \kappa\bar{K}_{32}^{(k)} & \kappa\bar{K}_{33}^{(k)} \end{bmatrix}, \qquad [\bar{K}_{ij}^{(k)}]_T = \begin{bmatrix} 0 & \bar{K}_{12}^{(k)} & 0 \\ 0 & \bar{K}_{22}^{(k)} & 0 \\ 0 & \bar{K}_{32}^{(k)} & 0 \end{bmatrix}, \tag{13, 14}$$

and κ is a Timoshenko shear coefficient (taken to be the same for both bending planes). It is a function of z and its value will be discussed later.

For the general case of an N-layered laminate (see Figure 4), one has

$$M_x = \sum_{k=1}^{N} \int_{A^{(k)}} y\sigma_z^{(k)}\,\mathrm{d}A.$$

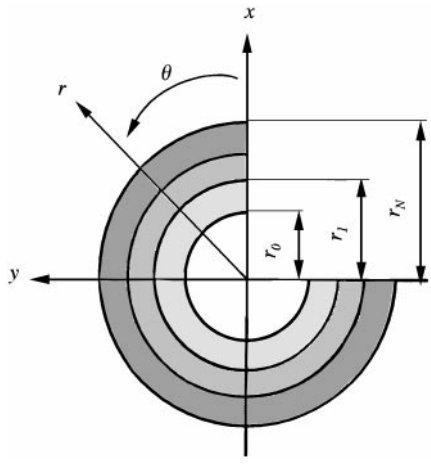

Figure 4. *N*-layered laminate.

Using equations (6)–(14) and noting the assumed axisymmetry of σ_r, σ_θ, integration leads to

$$M_x = K_M \psi'_y + \kappa K^s_{MV}(u'_y + \psi_y) - \kappa K^o_{MV}(u'_x - \psi_x), \tag{15}$$

where

$$K_M \text{ (bending coefficient)} = \sum_{k=1}^{N} \bar{K}^{(k)}_{11} \left\{ \frac{\pi}{4}(r_k^4 - r_{k-1}^4) \right\}, \tag{16}$$

K^s_{MV} (bending–shear (in the same direction) coupling coefficient)

$$= \sum_{k=1}^{N} \bar{K}^{(k)}_{13} \left\{ \frac{\pi}{3}(r_k^3 - r_{k-1}^3) \right\}, \tag{17}$$

K^o_{MV} (bending–shear (in the other direction) coupling coefficient)

$$= \sum_{k=1}^{N} \bar{K}^{(k)}_{12} \left\{ \frac{\pi}{3}(r_k^3 - r_{k-1}^3) \right\}. \tag{18}$$

Similarly, one finds

$$M_y = K_M \psi'_x - \kappa K^s_{MV}(u'_x - \psi_x) - \kappa K^o_{MV}(u'_y + \psi_y), \tag{19}$$

$$T = K_T \phi' + K_{TP} u'_z + K_{T\Omega}, \tag{20}$$

$$V_x = \kappa K^s_V(u'_x - \psi_x) + \kappa K^o_V(u'_y + \psi_y) - K^s_{VM}\psi'_x - K^o_{VM}\psi'_y, \tag{21}$$

$$V_y = \kappa K^s_V(u'_y + \psi_y) - \kappa K^o_V(u'_x - \psi_x) + K^s_{VM}\psi'_y - K^o_{VM}\psi'_x, \tag{22}$$

$$P = K_P u'_z + K_{PT}\phi' + K_{P\Omega}, \tag{23}$$

where

$$K_V^s(\text{shear coefficient}) = \sum_{k=1}^{N} \left(\frac{\bar{K}_{22}^{(k)} + \bar{K}_{33}^{(k)}}{2} \right) \{\pi (r_k^2 - r_{k-1}^2)\}, \tag{24}$$

$$K_V^o(\text{shear–shear coupling coefficient}) = \sum_{k=1}^{N} \left(\frac{\bar{K}_{32}^{(k)} - \bar{K}_{23}^{(k)}}{2} \right) \{\pi (r_k^2 - r_{k-1}^2)\}, \tag{25}$$

$$K_{VM}^s(\text{shear–bending (in the same direction) coupling coefficient}) = \sum_{k=1}^{N} \bar{K}_{31}^{(k)} \left\{ \frac{\pi}{3} (r_k^3 - r_{k-1}^3) \right\}, \tag{26}$$

$$K_{VM}^o(\text{shear–bending (in the other direction) coupling coefficient}) = \sum_{k=1}^{N} \bar{K}_{21}^{(k)} \left\{ \frac{\pi}{3} (r_k^3 - r_{k-1}^3) \right\}, \tag{27}$$

$$K_T(\text{torsion coefficient}) = \sum_{k=1}^{N} \bar{K}_{22}^{(k)} \left\{ \frac{\pi}{2} (r_k^4 - r_{k-1}^4) \right\}, \tag{28}$$

$$K_{TP}(\text{torsion–extension coupling coefficient}) = \sum_{k=1}^{N} \bar{K}_{21}^{(k)} \left\{ \frac{2\pi}{3} (r_k^3 - r_{k-1}^3) \right\}, \tag{29}$$

$$K_{T\Omega}(\text{torsion–rotation } (\Omega) \text{ coefficient}) = 2\pi \sum_{k=1}^{N} \int_{r_{k-1}}^{r_k} r^2 (\bar{C}_{21}^{(k)} \sigma_r^{(k)} + \bar{C}_{22}^{(k)} \sigma_\theta^{(k)}) \, \mathrm{d}r, \tag{30}$$

$$K_P(\text{extension coefficient}) = \sum_{k=1}^{N} \bar{K}_{11}^{(k)} \{\pi (r_k^2 - r_{k-1}^2)\}, \tag{31}$$

$$K_{PT}(\text{extension–torsion coupling coefficient}) = \sum_{k=1}^{N} \bar{K}_{12}^{(k)} \left\{ \frac{2\pi}{3} (r_k^3 - r_{k-1}^3) \right\}, \tag{32}$$

$$K_{P\Omega}(\text{extension–rotation } (\Omega) \text{ coefficient}) = 2\pi \sum_{k=1}^{N} \int_{r_{k-1}}^{r_k} r (\bar{C}_{11}^{(k)} \sigma_r^{(k)} + \bar{C}_{12}^{(k)} \sigma_\theta^{(k)}) \, \mathrm{d}r. \tag{33}$$

In Timoshenko beam theory, rotatory inertia is accounted for by treating a differential element (length $\mathrm{d}z$) as if it were a thin rigid disk rotating with Ω (about the z-axis) and the derivatives of the bending slopes $\dot{\psi}_x$, $\dot{\psi}_y$. Using the small-angle approximations $\cos\psi_x$, $\cos\psi_y \approx 1$, $\sin\psi_x \approx \psi_x$, $\sin\psi_y \approx \psi_y$ it can be shown that the moment $\bar{M}$ about the center of the disk is given by ($\mathbf{i}$, $\mathbf{j}$ and $\mathbf{k}$ denote unit vector along the x-, y- and z- axis, respectively)

$$\bar{M} = \{(I_x \ddot{\psi}_y + I_z \Omega \dot{\psi}_x)\mathbf{i} + (I_y \ddot{\psi}_x - I_z \Omega \dot{\psi}_y)\mathbf{j} + (I_z \ddot{\phi})\mathbf{k}\} \, \mathrm{d}z. \tag{34}$$

The inertia force $\bar{F}$ of the center of disk is given by

$$\bar{\mathbf{F}} = \{(m\ddot{u}_x)\mathbf{i} + (m\ddot{u}_y)\mathbf{j} + (m\ddot{u}_z)\mathbf{k}\}\,\mathrm{d}z. \tag{35}$$

In these expressions, I_x, I_y and I_z denote mass moments of inertia per unit length and m is the mass per unit length. Allowing the inclusion of a discrete mass, m_c, and mass moment of inertia, I_c, at $z = z_c$, these quantities are given by

$$I_x = I_y = \tfrac{1}{2}I_z = I_o + I_c\delta(z - z_c), \qquad m = m_o + m_c\delta(z - z_c), \tag{36, 37}$$

$$I_o = \sum_{k=1}^{N} \rho^{(k)} \left\{\frac{\pi}{4}(r_k^4 - r_{k-1}^4)\right\}, \qquad m_o = \sum_{k=1}^{N} \rho^{(k)}\{\pi(r_k^2 - r_{k-1}^2)\}, \tag{38, 39}$$

where $\rho^{(k)}$ is the layerwise mass density (as given by the rule of mixtures) and δ denotes the Dirac delta function. Using equations (15), (19)–(23), (34) and (35), the equilibrium of a differential element can be shown to lead to

$$\begin{aligned} L_1(u_x, u_y, \psi_x, \psi_y) \equiv{}& m\ddot{u}_x - \{\kappa K_V^s(u_x' + \psi_x)\}' + \{\kappa K_V^o(u_y' + \psi_y)\}' + \{K_{VM}^s\psi_x'\}' \\ &+ \{K_{VM}^o\psi_{xy}'\}' - f_x = 0, \end{aligned} \tag{40}$$

$$\begin{aligned} L_2(u_x, u_y, \psi_x, \psi_y) \equiv{}& m\ddot{u}_y - \{\kappa K_V^s(u_y' + \psi_y)\}' + \{\kappa K_V^o(u_x' - \psi_y)\}' - \{K_{VM}^s\psi_y'\}' \\ &+ \{K_{VM}^o\psi_x'\}' - f_y = 0, \end{aligned} \tag{41}$$

$$\begin{aligned} L_3(u_x, u_y, \psi_x, \psi_y) \equiv{}& I_y\ddot{\psi}_x - I_z\Omega\dot{\psi}_y - \{K_M\psi_x'\}' + \{\kappa K_{MV}^s(u_x' - \psi_x)\}' \\ &+ \{\kappa K_{MV}^o(u_y' + \psi_y)\}' - \kappa K_V^s(u_x' - \psi_x) - \kappa K_V^o(u_y' + \psi_y) \\ &+ K_{VM}^s\psi_x' + K_{VM}^o\psi_y' = 0, \end{aligned} \tag{42}$$

$$\begin{aligned} L_4(u_x, u_y, \psi_x, \psi_y) \equiv{}& I_x\ddot{\psi}_y + I_z\Omega\dot{\psi}_x - \{K_M\psi_y'\}' - \{\kappa K_{MV}^s(u_y' + \psi_y)\}' \\ &+ \{\kappa K_{MV}^o(u_x' - \psi_x)\}' + \kappa K_V^s(u_y' + \psi_y) - \kappa K_V^o(u_x' - \psi_x) \\ &+ K_{VM}^s\psi_y' - K_{VM}^o\psi_x' = 0, \end{aligned} \tag{43}$$

$$L_5(u_z, \phi) \equiv m\ddot{u}_z - (K_P u_z')' - (K_{PT}\phi')' - (K_{P\Omega})' - f_z = 0, \tag{44}$$

$$L_6(u_z, \phi) \equiv I_z\ddot{\phi} - (K_T\phi')' - (K_{TP}u_z')' - (K_{T\Omega})' - t_z = 0, \tag{45}$$

where f_x, f_y and f_z are applied forces per unit length and t_z is an applied torque per unit length. Note that the bending motions are coupled through gyroscopic effects and material effects, but are not coupled to extensional and torsional motions,

whereas the latter two are coupled only by material effects. Note also that σ_r and σ_θ have not, as yet, been specified. However, due to their assumed axisymmetry they influence only $K_{T\Omega}$ and $K_{P\Omega}$ [see equations (30) and (33)], which, as equations (44) and (45) show, in turn influence only the *forced* extensional and torsional responses. This issue will be addressed in a subsequent paper [15].

The shaft is taken to be clamped-free, the boundary conditions for which are

$$u_x(0) = u_y(0) = \psi_x(0) = \psi_y(0) = 0, \qquad u_z(0) = \phi(0) = 0, \tag{46, 47}$$

$$B_1(u_x, u_y, \psi_x, \psi_y) \equiv \kappa(L)K_V^s(L)\{u_x'(L) - \psi_x(L)\} + \kappa(L)K_V^o(L)\{u_y'(L) + \psi_y(L)\}$$
$$- K_{VM}^s(L)\psi_x'(L) - K_{VM}^o(L)\psi_y'(L) = 0, \tag{48}$$

$$B_2(u_x, u_y, \psi_x, \psi_y) \equiv \kappa(L)K_V^s(L)\{u_y'(L) + \psi_y(L)\} - \kappa(L)K_V^o(L)\{u_x'(L) - \psi_x(L)\}$$
$$+ K_{VM}^s(L)\psi_y'(L) - K_{VM}^o(L)\psi_x'(L) = 0, \tag{49}$$

$$B_3(u_x, u_y, \psi_x, \psi_y) \equiv K_M(L)\psi_x'(L) - \kappa(L)K_{MV}^s(L)\{u_x'(L) - \psi_x(L)\}$$
$$- \kappa(L)K_{MV}^o(L)\{u_y'(L) + \psi_y(L)\} = 0, \tag{50}$$

$$B_4(u_x, u_y, \psi_x, \psi_y) \equiv K_M(L)\psi_y'(L) + \kappa(L)K_{MV}^s(L)\{u_y'(L) + \psi_y(L)\}$$
$$- \kappa(L)K_{MV}^o(L)\{u_x'(L) - \psi_x(L)\} = 0, \tag{51}$$

$$B_5(u_z, \phi) \equiv K_P(L)u_z'(L) + K_{PT}(L)\phi'(L) + K_{P\Omega}(L) = 0, \tag{52}$$

$$B_6(u_z, \phi) \equiv K_T(L)\phi'(L) + K_{TP}(L)u_z'(L) + K_{T\Omega}(L) = 0. \tag{53}$$

3. GENERAL GALERKIN METHOD

Analytic solutions to equations (40)–(45) are not feasible and here recourse is made to Galerkin's method. One takes

$$u_x = \sum_{n=1}^{N_G} A_n^{(x)}(t)\,\xi_n(z), \qquad u_y = \sum_{n=1}^{N_G} A_n^{(y)}(t)\,\xi_n(z), \tag{54, 55}$$

$$\psi_x = \sum_{n=1}^{N_G} B_n^{(x)}(t)\,\alpha_n(z), \qquad \psi_y = \sum_{n=1}^{N_G} B_n^{(y)}(t)\,\alpha_n(z), \tag{56, 57}$$

$$u_z = \sum_{n=1}^{N_G} C_n(t)\,\eta_n(z), \qquad \phi = \sum_{n=1}^{N_G} D_n(t)\,\varphi_n(z). \tag{58, 59}$$

The Galerkin functions, ξ_n, for the bending variables u_x and u_y are taken to be the mode shapes of a uniform, non-rotating, isotropic, fixed-free Euler–Bernoulli beam, namely

$$\xi_n = (\sin \beta_n z - \sinh \beta_n z) + \frac{(\cos \beta_n L + \cosh \beta_n L)}{(\sin \beta_n L - \sinh \beta_n L)} (\cos \beta_n z - \cosh \beta_n z), \quad (60)$$

where β_n is obtained from

$$\cos \beta_n L \cosh \beta_n L + 1 = 0. \quad (61)$$

The Galerkin functions, α_n, for the angular deformations ψ_x and ψ_y are taken to be

$$\alpha_n = \sin \frac{(2n-1)\pi z}{2L}. \quad (62)$$

Note that ξ_n and α_n satisfy the geometric boundary conditions of the problem, as given by equation (46).

The extensional and torsional Galerkin functions are taken as

$$\eta_n = \sin \frac{(2n-1)\pi z}{2L}, \qquad \varphi_n = \sin \frac{(2n-1)\pi z}{2L} \quad (63, 64)$$

which satisfy the geometric boundary conditions given by equation (47).

The Galerkin functions chosen do not satisfy the boundary conditions given by equations (48)–(53) and so the general Galerkin method is employed here (see Leipholz [16]). In this method, boundary residuals as well as differential equation residuals are treated as follows.

Substituting equations (54)–(57) into equation (40) gives an expression of the form

$$L_1 \left(\sum_{n=1}^{N_G} A_n^{(x)} \xi_n, \quad \sum_{n=1}^{N_G} A_n^{(y)} \xi_n, \quad \sum_{n=1}^{N_G} B_n^{(x)} \alpha_n, \quad \sum_{n=1}^{N_G} B_n^{(y)} \alpha_n \right) = 0. \quad (65)$$

Multiplying this by ξ_m and integrating from 0 to L gives

$$R_{1m} \equiv \int_0^L \xi_m L_1 \, \mathrm{d}z. \quad (66)$$

The associated boundary condition (48) is handled by substituting equations (54)–(57) in equation (48) and then multiplying by $\xi_m(L)$, giving the boundary residual

$$R_{1Bm} \equiv \xi_m(L) B_1 \left(\sum_{n=1}^{N_G} A_n^{(x)} \xi_n(L), \sum_{n=1}^{N_G} A_n^{(y)} \xi_n(L), \sum_{n=1}^{N_G} B_n^{(x)} \alpha_n(L), \sum_{n=1}^{N_G} B_n^{(y)} \alpha_n(L) \right). \quad (67)$$

In the general Galerkin method, one takes

$$R_{1m} + R_{1Bm} = 0, \quad m = 1, 2, \ldots, N_G. \tag{68}$$

Similarly, the remaining equations give

$$\begin{aligned} &R_{2m} + R_{2Bm} = 0, \quad R_{3m} + R_{3Bm} = 0, \quad R_{4m} + R_{4Bm} = 0, \\ &R_{5m} + R_{5Bm} = 0, \quad R_{6m} + R_{6Bm} = 0, \end{aligned} \qquad m = 1, 2, \ldots, N_G, \tag{69–73}$$

where

$$R_{2m} \equiv \int_0^L \xi_m L_2 \, \mathrm{d}z, \quad R_{3m} \equiv \int_0^L \alpha_m L_3 \, \mathrm{d}z, \quad R_{4m} \equiv \int_0^L \alpha_m L_4 \, \mathrm{d}z, \tag{74–76}$$

$$R_{5m} \equiv \int_0^L \eta_m L_5 \, \mathrm{d}z, \quad R_{6m} \equiv \int_0^L \varphi_m L_6 \, \mathrm{d}z, \tag{77, 78}$$

$$R_{2Bm} \equiv \xi_m(L) B_2 \left(\sum_{n=1}^{N_G} A_n^{(x)} \xi_n(L), \sum_{n=1}^{N_G} A_n^{(y)} \xi_n(L), \sum_{n=1}^{N_G} B_n^{(x)} \alpha_n(L), \sum_{n=1}^{N_G} B_n^{(y)} \alpha_n(L) \right), \tag{79}$$

$$R_{3Bm} \equiv \alpha_m(L) B_3 \left(\sum_{n=1}^{N_G} A_n^{(x)} \xi_n(L), \sum_{n=1}^{N_G} A_n^{(y)} \xi_n(L), \sum_{n=1}^{N_G} B_n^{(x)} \alpha_n(L), \sum_{n=1}^{N_G} B_n^{(y)} \alpha_n(L) \right), \tag{80}$$

$$R_{4Bm} \equiv \alpha_m(L) B_4 \left(\sum_{n=1}^{N_G} A_n^{(x)} \xi_n(L), \sum_{n=1}^{N_G} A_n^{(y)} \xi_n(L), \sum_{n=1}^{N_G} B_n^{(x)} \alpha_n(L), \sum_{n=1}^{N_G} B_n^{(y)} \alpha_n(L) \right), \tag{81}$$

$$R_{5Bm} \equiv \eta_m(L) B_5 \left(\sum_{n=1}^{N_G} C_n \eta_n(L), \sum_{n=1}^{N_G} D_n \varphi_n(L) \right), \tag{82}$$

$$R_{6Bm} \equiv \varphi_m(L) B_6 \left(\sum_{n=1}^{N_G} C_n \eta_n(L), \sum_{n=1}^{N_G} D_n \varphi_n(L) \right). \tag{83}$$

The end product of the procedure is a set of equations of the form

$$[M_1] \begin{Bmatrix} \{\ddot{A}_n^{(x)}\} \\ \{\ddot{A}_n^{(y)}\} \\ \{\ddot{B}_n^{(x)}\} \\ \{\ddot{B}_n^{(y)}\} \end{Bmatrix} + [G_1] \begin{Bmatrix} \{\dot{A}_n^{(x)}\} \\ \{\dot{A}_n^{(y)}\} \\ \{\dot{B}_n^{(x)}\} \\ \{\dot{B}_n^{(y)}\} \end{Bmatrix} + [K_1] \begin{Bmatrix} \{A_n^{(x)}\} \\ \{A_n^{(y)}\} \\ \{B_n^{(x)}\} \\ \{B_n^{(y)}\} \end{Bmatrix} = \{F_1\}, \tag{84}$$

$$[M_2] \begin{Bmatrix} \{\ddot{C}_n\} \\ \{\ddot{D}_n\} \end{Bmatrix} + [K_2] \begin{Bmatrix} \{C_n\} \\ \{D_n\} \end{Bmatrix} = \{F_2\}, \tag{85}$$

where

$$[M_1] = \begin{bmatrix} [M_A] & [0] & [0] & [0] \\ [0] & [M_A] & [0] & [0] \\ [0] & [0] & [M_B] & [0] \\ [0] & [0] & [0] & [M_B] \end{bmatrix}, \quad [G_1] = \begin{bmatrix} [0] & [0] & [0] & [0] \\ [0] & [0] & [0] & [0] \\ [0] & [0] & [0] & [-G_B] \\ [0] & [0] & [G_B] & [0] \end{bmatrix},$$

$$[K_1] = \begin{bmatrix} [K_A^s] & [K_A^o] & [-K_{AB}^s] & [K_{AB}^o] \\ [-K_A^o] & [K_A^s] & [K_{AB}^o] & [K_{AB}^s] \\ [-K_{BA}^s] & [K_{BA}^o] & [K_B^s] & [K_B^o] \\ [K_{BA}^o] & [K_{BA}^s] & [-K_B^o] & [K_B^s] \end{bmatrix}, \quad [M_2] = \begin{bmatrix} [M_C] & [0] \\ [0] & [M_D] \end{bmatrix},$$

$$[K_2] = \begin{bmatrix} [K_C] & [K_{CD}] \\ [K_{DC}] & [K_D] \end{bmatrix}. \tag{86–90}$$

The elements of the matrices in equations (86)–(90) are given in Appendix B. The force-like terms in equations (84) and (85) are given by

$$\{F_1\} = \begin{Bmatrix} \{f_n^{(x)}\} \\ \{f_n^{(y)}\} \\ \{0\} \\ \{0\} \end{Bmatrix}, \qquad \{F_2\} = \begin{Bmatrix} \{f_n^{(z)}\} \\ \{t_n^{(z)}\} \end{Bmatrix}. \tag{91, 92}$$

where

$$f_n^{(x)} = \int_0^L f_x \xi_n \, \mathrm{d}z, \quad f_n^{(y)} = \int_0^L f_y \xi_n \, \mathrm{d}z, \quad f_n^{(z)} = \int_0^L (f_z \eta_n - K_{P\Omega} \eta_n') \, \mathrm{d}z,$$

$$t_n^{(z)} = \int_0^L (t_z \varphi_n - K_{T\Omega} \varphi_n') \, \mathrm{d}z. \tag{93–96}$$

4. NUMERICAL RESULTS

At this stage, a choice has to be made on how the Timoshenko shear coefficients are to be determined. There are numerous schemes in the literature for their determination. The approach adopted here is based on that of Dharmarajan and McCutchen [17] who, generalizing Cowper's method [18], showed that for an orthotropic, hollow circular beam (inner radius a, outer radius b), κ is given by

$$\kappa = \frac{6E_{zz}(1 - \bar{m}^4)(1 + \bar{m}^2)}{G_{zx}\nu_{zx}(2\bar{m}^6 + 18\bar{m}^4 - 18\bar{m}^2 - 2) - E_{zz}(7\bar{m}^6 + 27\bar{m}^4 - 27\bar{m}^2 - 7)}, \tag{97}$$

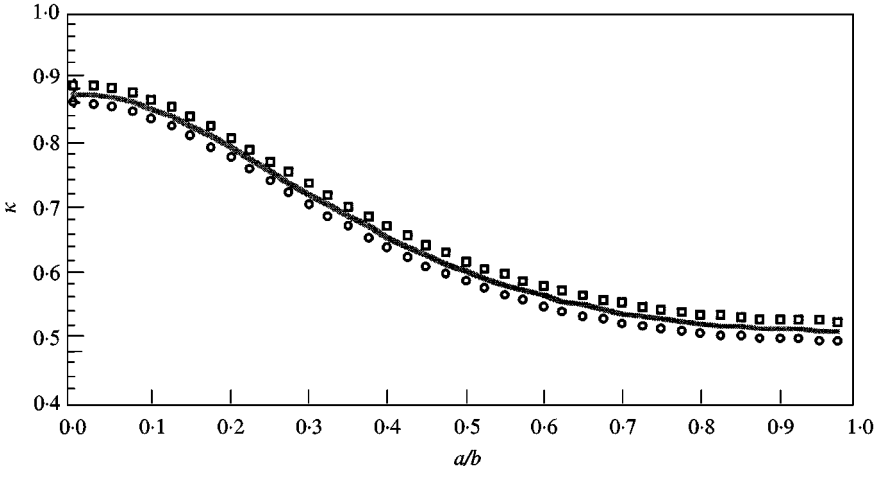

Figure 5. Timoshenko shear coefficient versus a/b ratio: □, κ_{steel}; ○, $\kappa_{composite}$; ——, $\kappa_{average}$.

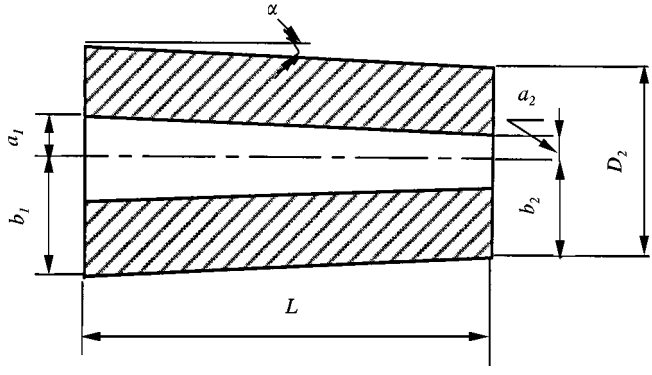

Figure 6. Linearly tapered hollow shafts: $\alpha = 1{\cdot}7°$, $b_1 - a_1 = 5{\cdot}4$ mm, $a_2 = 1$ mm, $b_2 = D_2/2 = 6{\cdot}4$ mm; rotational speed = 400 rad/s.

where $\bar{m} = a/b$. (The bold-faced sign in equation (97) is minus in reference [17] which we believe to be a typographical error. Also, to be consistent with our notation, we have replaced their v_{xz} by v_{zx}.) For composite material (0° high modulus graphite/epoxy) and steel, a plot of κ, as given by equation (97), versus a/b is given in Figure 5. In this figure, the solid line is the average Timoshenko shear coefficient, $\kappa_{average}$, of $\kappa_{composite}$ and κ_{steel}. The properties of the composite are (obtained from reference [19]): $E_{zz} = 192$ GPa, $G_{zx} = 4{\cdot}07$ GPa, $v_{zx} = 0{\cdot}24$.

Consider numerical examples involving a linear taper as illustrated in Figure 6. The bending natural frequencies are obtained from the homogeneous version of equation (84). When a beam rotates, each non-rotating bending frequency branches into two. In the sequel, "lowest bending frequency" refers to the smaller of these two frequencies. The lowest bending frequency, as determined by both Timoshenko and Rayleigh beam theories, of the composite (0°) shaft as a function of the L/D_2 ratio is shown in Table 1. Three Galerkin functions were used and found to be sufficient for

TABLE 1

The lowest bending frequency (Hz) *of the composite* (0°) *shaft*

L/D_2 ratio	$\kappa = \kappa_{average}$	$\kappa = \kappa_{composite}$	$\kappa = \kappa_{steel}$	Rayleigh
5	4900·5	4870·6 (−0·61%)	4929·0 (0·58%)	7009·3 (43·0%)
10	1983·9	1976·3 (−0·38%)	1991·2 (0·37%)	2340·5 (18·0%)
20	824·5	822·5 (−0·24%)	826·4 (0·23%)	898·2 (8·9%)

TABLE 2

The lowest bending frequency (Hz) *of the composite* (20°) *shaft*

L/D_2 ratio	$\kappa = \kappa_{average}$	$\kappa = \kappa_{composite}$	$\kappa = \kappa_{steel}$	Rayleigh
5	3392·8	3382·9 (−0·29%)	3402·3 (0·28%)	5360·0 (58·0%)
10	1198·2	1196·2 (−0·17%)	1200·1 (0·16%)	1789·7 (49·4%)
20	462·5	461·9 (−0·13%)	463·0 (0·11%)	686·8 (48·5%)

TABLE 3

The lowest bending frequency (Hz) *of the steel shaft*

L/D_2 ratio	$\kappa = \kappa_{average}$	$\kappa = \kappa_{composite}$	$\kappa = \kappa_{steel}$	Rayleigh
5	3199·4	3197·2 (−0·07%)	3201·5 (0·07%)	3331·4 (4·1%)
10	1093·6	1093·3 (−0·03%)	1094·0 (0·04%)	1112·3 (1·7%)
20	423·4	423·3 (−0·02%)	423·5 (0·02%)	426·9 (0·8%)

convergence. To assess sensitivity of the frequency to the choice of κ, the three values of κ seen in Figure 5 were used, namely $\kappa_{composite}$, κ_{steel} and $\kappa_{average}$ for all cases. Note that κ is a function of z because the a/b ratio is varying along the z-axis. As shown in Table 1, the natural frequency values are to a large degree insensitive to the choice of κ. At $L/D_2 = 5$, the frequencies differ by $-0{\cdot}61\%$ ($\kappa = \kappa_{composite}$) and $0{\cdot}58\%$ ($\kappa = \kappa_{steel}$) compared to the $\kappa = \kappa_{average}$ case. These drop to $-0{\cdot}24\%$ ($\kappa = \kappa_{composite}$) and $0{\cdot}23\%$ ($\kappa = \kappa_{steel}$) at $L/D_2 = 20$. Similar results for the composite (20°) shaft and the steel shaft are shown in Tables 2 and 3 respectively.

Some comments should be made about Table 2 since it contains results for generally orthotropic shafts. To the authors' knowledge no result like equation (97) valid for more general anisotropy is available. Teh and Huang [20] considered general rectilinear orthotropy. They showed that the difference in κ between 0° and 90° was less than 1% for graphite/epoxy. In Table 2, the anisotropy is curvilinear but it is still assumed that κ as given by the 0° case [equation (97)] holds for all configurations.

In the light of the foregoing results, it is felt that the results are insensitive to the choice of κ within an acceptable level of accuracy. With this in mind the strategy used is as follows. Figure 5 shows that the dependence of κ on material values plays

a secondary role to the geometry, so the same value of κ, namely, $\kappa_{average}$, is used for all layers even though different materials and fibre angles are used.

A point to be noted from these tables is that the differences between the Timoshenko and Rayleigh beam theories for $L/D_2 = 5$ are 43% for 0° composite, 58% for 20° composite and 4·1% for steel. These drop to 8·9% (0° composite), 48·5% (20° composite) and 0·8% (steel) at $L/D_2 = 20$. The large shear effect that occurs in the 20° composite case even for the large ($L/D_2 = 20$) slenderness ratio is due to coupling between bending in the xz-plane and shearing in the yz-plane (i.e., γ_{yz}) that exists for this shaft.

Some results regarding the lowest natural frequencies and the static stiffnesses for bending and torsion will now be presented for various taper versions of the three equivolume shafts described in Figure 7. All shafts have the same length and thickness. The tapers are linear and $L/(b_1 + b_2) = 12$. The lowest non-dimensional bending frequency (ω_b) is shown in Figure 8(a) as a function of the taper ratio $[TR = 100(b_1 - b_2)/L]$. Non-dimensionalization (bending, torsional as appropriate) is achieved by dividing by the lowest value for the zero taper ratio case. The rotational speed is 400 rad/s. It is seen that the frequencies can be increased by the use of composite materials. This increase would be beneficial for rotational speeds operating below the lowest natural frequency. Another way to view this benefit is as follows. Consider a non-tapered shaft operating at a certain frequency. By the use of composite materials, a shaft can be made with the same frequency and diameter, but with a greater length. This increase in length is beneficial in that it allows a wider range of applications. Figure 8 also shows that tapering increases the frequencies. Thus, tapered shafts having the same frequency but smaller diameter (over a portion of their length) than non-tapered shafts can be designed. This also results in a wider range of applications. In all four cases, the frequencies at a taper ratio of 3 are increased by approximately 70% compared with the uniform ($TR = 0$) case. Also, all shafts containing composite materials show increased bending frequency and reduced mass compared to the steel shaft. For example, at taper ratio 2, the steel/0° composite shaft results in a 41% higher frequency than the pure steel shaft, while reducing the mass by 50%. Similar trends are seen in Figure 8(b) for cases having $L/(b_1 + b_2) = 6$ (inner and outer radii are doubled, keeping the same length).

In Figures 8(a, b), dotted lines indicate results obtained from the Rayleigh beam theory for the hollow composite shaft. The differences between the Timoshenko and Rayleigh theories are approximately 5% for $L/(b_1 + b_2) = 12$. This is increased to 16% for $L/(b_1 + b_2) = 6$.

Some results on the effect of rotational speed will now be presented in the form of Campbell diagrams. Figures 9(a, b) show the first-mode bending frequency pairs as functions of rotational speed for a variety of cases. The composite layering and material properties are taken from Figure 7 and two length cases are treated: $L/(b_1 + b_2) = 12$—Figure 9(a) and $L/(b_1 + b_2) = 6$—Figure 9(b). Non-dimensionalization is achieved using the value (ω_s) of the steel shaft at $\Omega = 0$ [$\omega_s = 1735$ rad/s for $L/(b_1 + b_2) = 12$ and 3406 rad/s for $L/(b_1 + b_2) = 6$]. In general, if Ω is increased from 0, two natural frequencies occur for each mode. The higher value usually corresponds to a mode in which the shaft precesses in the same

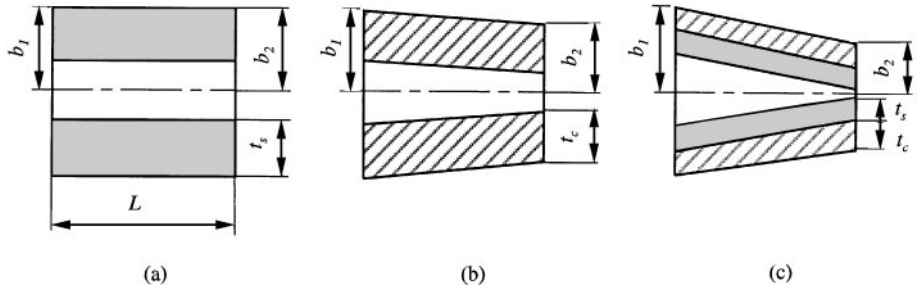

Figure 7. Simulation cases ($L/(b_1 + b_2) = 12$, $m_c = I_c = 0$): (a) hollow steel shaft (here shown non-tapered), mass = 458 g, length $L = 240$ mm, $t_s = 5{\cdot}4$ mm, $b_1 = b_2 = 10$ mm, material properties ($\rho = 7700$ kg/m^3, $E = 207$ GPa, $G = 80$ GPa); (b) hollow composite shaft [here shown having linear taper ratio (TR) $= 100(b_1 - b_2)/L = 2{\cdot}0$], 36 layers $(0_6/90_3/\pm 20_3/0_6/\mp 20_3/90_3/0_6)$, mass = 96 g, $L = 240$ mm, $t_c = 5{\cdot}4$ mm, $b_1 = 12{\cdot}4$ mm, $b_2 = 7{\cdot}6$ mm, high modulus graphite/epoxy ($\rho = 1610$ kg/m^3, $E_1 = 192$ GPa, $E_2 = 7{\cdot}24$ GPa, $G_{12} = 4{\cdot}07$ GPa, $G_{23} = 3{\cdot}0$ GPa, $\nu_{12} = 0{\cdot}24$); (c) composite shaft with steel core (here shown having $TR = 3{\cdot}0$), two 20 layer cases treated [$(0)_{20}$ and $(\pm 20)_{10}$], mass = 224 g, $L = 240$ mm, $t_c = 3$ mm, $t_s = 2{\cdot}4$ mm, $b_1 = 13{\cdot}6$ mm, $b_2 = 6{\cdot}4$ mm.

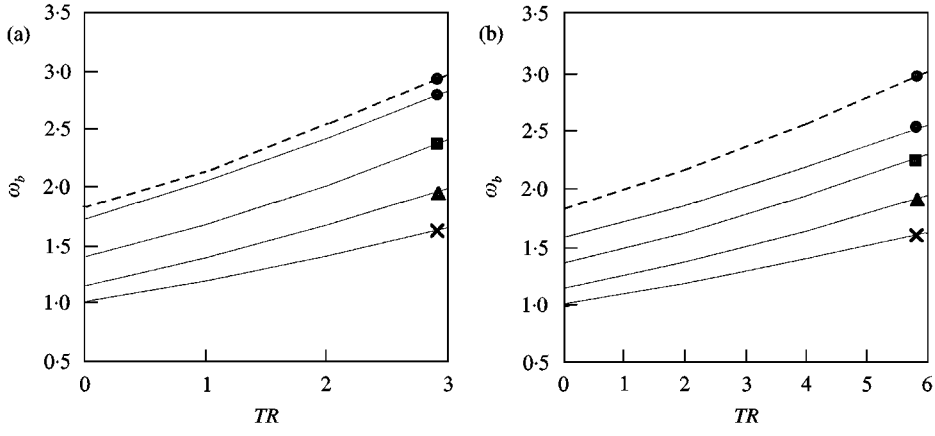

Figure 8. The lowest non-dimensional bending frequency versus taper ratio when (a) $L/(b_1 + b_2) = 12$ and (b) $L/(b_1 + b_2) = 6$: —, Timoshenko beam; - - - -, Rayleigh beam; ●, hollow composite: ■, steel/0° composite; ▲, steel/ $\pm$ 20° composite; ×, steel.

direction as the shaft's spin and so is called the forward precession. Likewise, the lower value usually represents a backward precessing mode. Note that the difference between forward and backward modes of the Timoshenko beam is slightly larger than that of Rayleigh beam. The differences at $\Omega = 15\,000$ rad/s [$\Omega/\omega_s = 8{\cdot}6$ in Figure 9(a)] are 2% (Timoshenko) and 0·4% (Rayleigh) for the non-tapered hollow composite shaft having $L/(b_1 + b_2) = 12$. These [at $\Omega/\omega_s = 4{\cdot}4$ in Figure 9(b)] are increased to 3% (Timoshenko) and 0·9% (Rayleigh) for $L/(b_1 + b_2) = 6$. For all Ω in the range 0–15 000 rad/s, the forward and backward modes of the shafts containing the composite are higher than the steel shaft modes. Also, it is seen that the tapered shaft ($TR = 3$) frequencies are higher than those of the uniform shaft ($TR = 0$) for the steel/ $\pm$ 20° composite case.

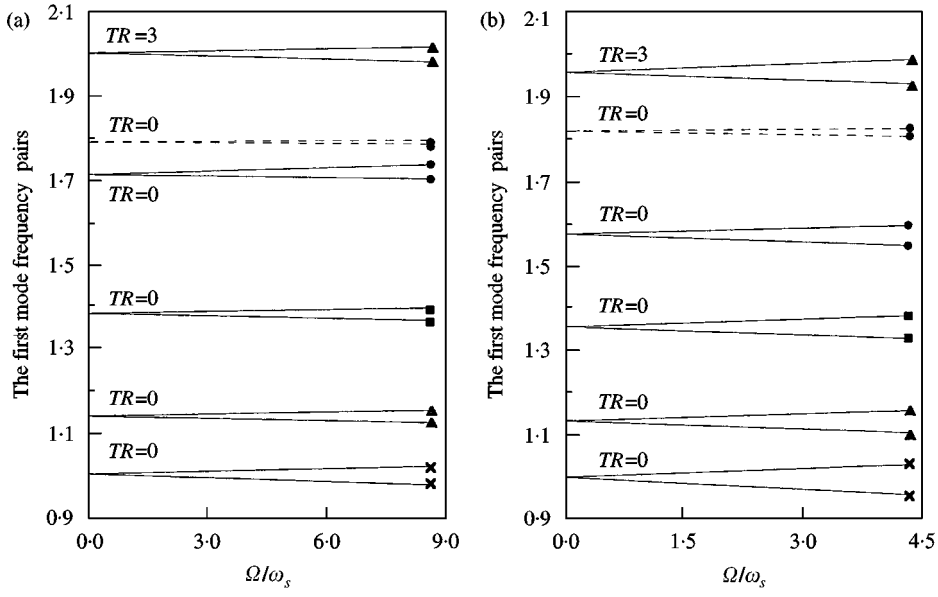

Figure 9. Campbell diagram when (a) $L/(b_1 + b_2) = 12$ and (b) $L/(b_1 + b_2) = 6$; —, Timoshenko beam; - - - -, Rayleigh beam; ●, hollow composite; ■, steel/0° composite; ▲, steel/ ± 20° composite; ×, steel.

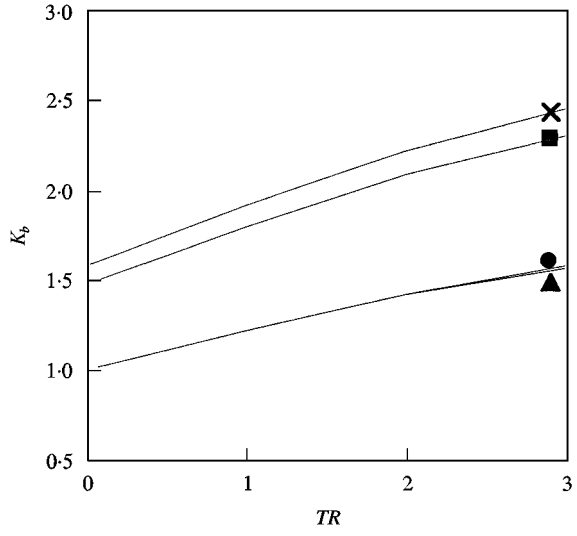

Figure 10. The non-dimensional static bending stiffness versus taper ratio when $L/(b_1 + b_2) = 12$; ●, hollow composite; ■, steel/0° composite; ▲, steel/ ± 20° composite; ×, steel.

The non-dimensional static bending stiffnesses (K_b), defined by the quotient of a point force at $z = L$ and the resulting static tip deflection, are shown in Figure 10. Another beneficial feature noted is that, the static bending stiffnesses are increased by shaft tapering in all cases. Bollinger [1] recorded that this trend can be beneficial for machining accuracy. The stiffness of the steel/0° composite shaft is slightly lower

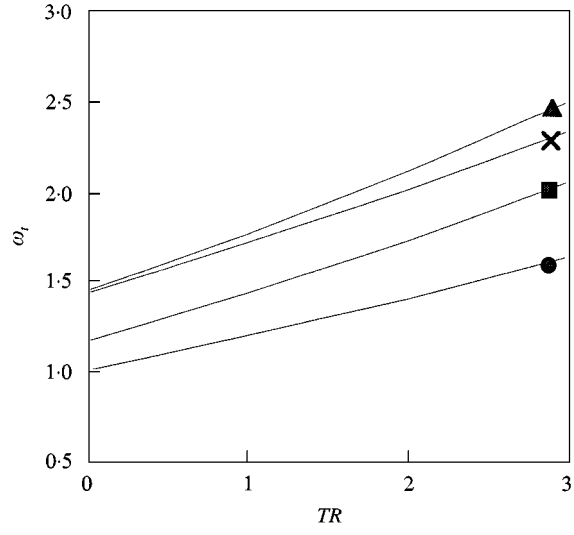

Figure 11. The lowest non-dimensional torsional frequency versus taper ratio when $L/(b_1 + b_2) = 12$; ●, hollow composite; ■, steel/0° composite; ▲, steel/ ± 20° composite; ×, steel.

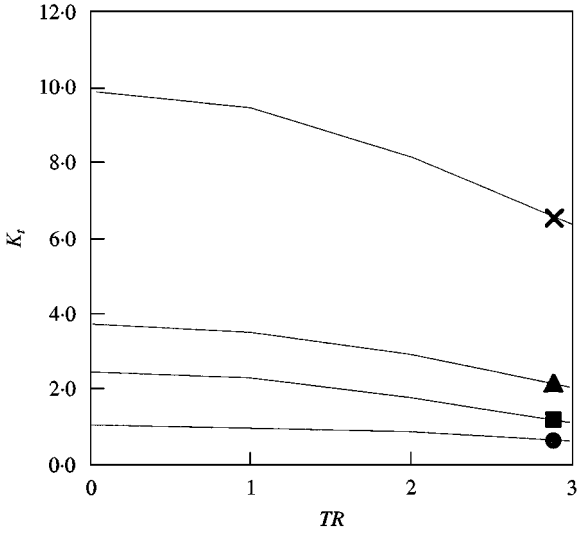

Figure 12. The non-dimensional static torsional stiffness versus taper ratio when $L/(b_1 + b_2) = 12$; ●, hollow composite; ■, steel/0° composite; ▲, steel/ ± 20° composite; ×, steel.

than that of the steel shaft; however, the mass of the steel/composite shaft is only one-half that of the steel shaft, as already noted.

Torsional natural frequencies can be obtained from the homogeneous version of equation (85). The lowest non-dimensional torsional frequency (ω_t) as a function of taper ratio is shown in Figure 11 for a rotational speed of 400 rad/s. Taper tends to increase the frequencies in all cases. The cases containing steel have higher natural frequencies than the pure composite case due to the high torsional modulus of steel;

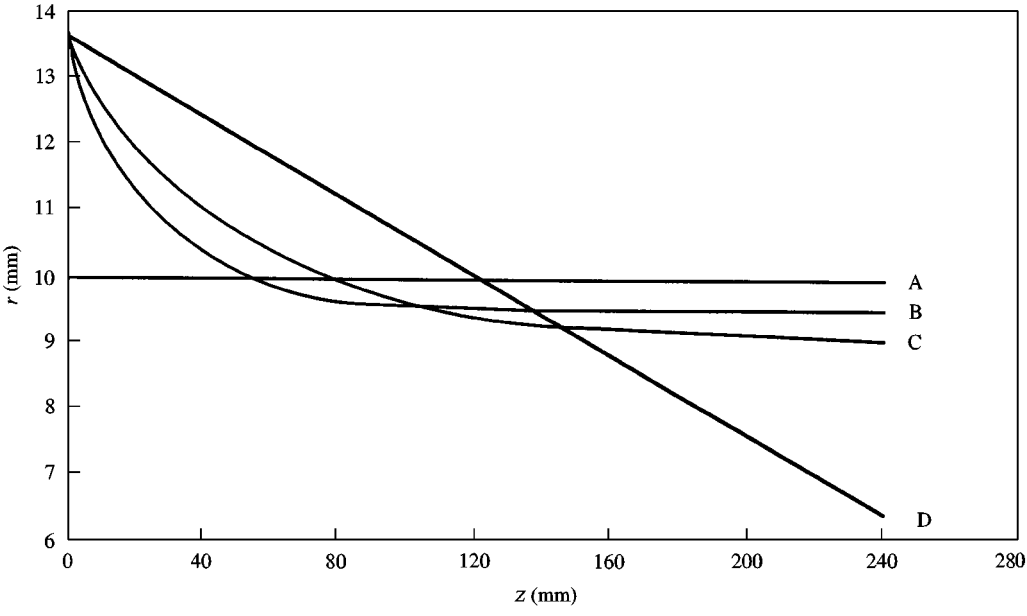

Figure 13. Outer radii of the non-tapered shaft A, the exponentially tapered shafts B and C, and the linearly tapered shaft D as functions of z.

however, the steel/$\pm 20^\circ$ composite case has the highest natural frequencies for all taper ratios. The non-dimensional static torsional stiffness (K_t), defined by the quotient of a point torque at $z = L$ and the resulting tip rotation, is shown in Figure 12. The torsional stiffness is decreased compared to steel by using composite material and also decreased by tapering. Whether such trends are detrimental or beneficial, and the overall roles of torsional stiffness and response on cutting accuracy are not clear from the literature (see references [21, 22], for example) and warrant further investigation.

Effects of exponential tapering were also studied. In Figure 13, comparisons are made between a non-tapered shaft A, a linearly tapered shaft D ($TR = 3$) and exponentially tapered shafts B and C. All four shafts are hollow composite ($0_6/90_3/\pm 20_3/0_6/\mp 20_3/90_3/0_6$) having the same length (240 mm), thickness (5·4 m), and volume (59 cm^3). The outer radii of shafts B and C are given by $(b_1 - b_2)e^{-sz} + b_2$, where $b_1 = 13{\cdot}6$ mm, $b_2 = 9{\cdot}52$ mm and $s = 40$ for shaft B, and $b_1 = 13{\cdot}6$ mm, $b_2 = 8{\cdot}99$ mm and $s = 20$ for shaft C. The non-dimensional static stiffnesses for bending (K_b) and torsion (K_t), the lowest non-dimensional bending frequency (ω_b), and the lowest non-dimensional torsional frequency (ω_t) are shown in Table 4. Non-dimensionalizations are achieved by dividing by the shaft A values. Convergence of the lowest natural frequencies necessitates five Galerkin functions for the exponentially tapered cases compared with three for the linearly tapered case. The frequencies and stiffness are seen to vary with the degree of tapering and lie between the non-tapered and linearly tapered values. A potential benefit to the use of exponential tapering lies in their inherent design flexibility. For example, in Figure 13, the portion of the shaft having a diameter smaller than the non-tapered

TABLE 4

Effects of exponential tapering

Shaft	Bending		Torsion	
	Frequency, ω_b	Stiffness, K_b	Frequency, ω_t	Stiffness, K_t
A	1·00	1·00	1·00	1·00
B	1·14	1·14	1·12	0·94
C	1·26	1·23	1·23	0·89
D	1·66	1·58	1·63	0·63

case is extended in the exponentially tapered cases compared to the linearly tapered case. Taper functions can be designed to extend this length to achieve specific internal cutting operations.

ACKNOWLEDGMENTS

This work was supported by the United States of America National Science Foundation grant number DMI-9522897 to the second author.

REFERENCES

1. J. G. BOLLINGER 1988 *Shock and Vibration Handbook* (C. M. Harris, editor), New York: McGraw-Hill, third edition. Machine-tool vibration, chapter 40.
2. K. Z. Y. YEN and W. C. HSUEH 1996 *JSME International Journal, Series C* **39**, 25–33. Suppression of chatter vibration in inner-diameter cutting.
3. D. B. RICHARDSON 1993 *Manufacturing Engineer's Reference Book* (D. Koshal, editor). Boston: Butterworth-Heinemann. Large-chip metal removal, chapter 5.
4. S. NAGANO, T. KOIZUMI, T. FUJII and N. TSUJIUCHI 1995 *27th International SAMPE Technical Conference* **27**, 397–408. Development of a CFRP boring bar.
5. A. TREGO, P. F. EASTMAN, W. F. PRATT and C. G. JENSEN 1995 *Design Engineering Technical Conference* (*ASME DE-Vol. 84-1*) **3**, part A, 305–310. Reduced boring bar vibrations using damped composite structures.
6. A. ARGENTO, H. L. MORANO and R. A. SCOTT 1994 *Journal of Vibration and Acoustics* **116**, 397–403. Accelerating load on a rotating Rayleigh beam.
7. K. E. ROUCH and J.-S. KAO 1979 *Journal of Sound and Vibration* **66**, 119–140. A tapered beam finite element for rotor dynamics analysis.
8. G. GENTA and A. GUGLIOTTA 1988 *Journal of Sound and Vibration* **120**, 175–182. A conical element for finite element rotor dynamics.
9. C. J. MADAY 1974 *Journal of Engineering for Industry* **96**, 166–170. A class of minimum weight shafts.
10. C. W. BERT and C.-D. KIM 1995 *Journal of Vibration and Acoustics* **117**, 17–21. Whirling of composite-material driveshafts including bending-twisting coupling and transverse shear deformation.
11. O. SONG and L. LIBRESCU 1997 *Journal of Sound and Vibration* **204**, 477–494. Anisotropy and structural coupling on vibration and instability of spinning thin-walled beams.

12. O. Song, N.-H. Jeong and L. Librescu 1997 *Collection of Technical Papers-AIAA/ASME/ASCE/AHS/ASC Structures, Structural Dynamics & Materials Conference (AIAA 97-1091)* **1**, 312–322. New York: AIAA. Modeling and vibration of pretwisted spinning composite thin-walled beams.
13. O. A. Bauchau 1983 *Journal of Composite Materials* **17**, 170–181. Optimal design of high speed rotating graphite/epoxy shafts.
14. R. M. Jones 1975 *Mechanics of Composite Materials*, Washington: Scripta Book Co., chapter 2.
15. W. Kim, A. Argento and R. A. Scott *Journal of Vibration and Acoustics*. Rotating, tapered composite shafts: forced torsional and extensional motions and static strength. (to be submitted).
16. H. Leipholz 1987 *Stability Theory: An Introduction to the Stability of Dynamic Systems and Rigid Bodies*, 120–135. New York: John Wiley & Sons, second edition.
17. S. Dharmarajan and H. McCutchen, Jr. 1973 *Journal of Composite Materials* **7**, 530–535. Shear coefficients for orthotropic beams.
18. G. R. Cowper 1966 *Journal of Applied Mechanics* **33**, 335–340. The shear coefficient in Timoshenko's beam theory.
19. J. P. Riggs 1990 *International Encylopedia of Composites* (S. M. Lee, editor), **1**, 197–222. New York: VCH Publishers. Carbon fibers.
20. K. K. Teh and C. C. Huang 1979 *Fibre Science and Technology* **12**, 73–80. Shear deformation coefficient for generally orthotropic beam.
21. E. I. Rivin and H. Kang 1992 *International Journal of Machine Tools & Manufacture* **32**, 539–561. Enhancement of dynamic stability of cantilever tooling structures.
22. G. M. Zhang and S. G. Kapoor 1987 *Journal of Engineering for Industry* **109**, 219–226. Dynamic modeling and analysis of the boring machining system.

APPENDIX A: MATRIX COEFFICIENTS, K_{ij}

$$K_{11} = \bar{Q}_{11}\sin^4\alpha + 2(\bar{Q}_{13} + 2\bar{Q}_{55})\sin^2\alpha\cos^2\alpha + \bar{Q}_{33}\cos^4\alpha,$$

$$K_{12} = \bar{Q}_{12}\sin^2\alpha + \bar{Q}_{23}\cos^2\alpha,$$

$$K_{13} = \bar{Q}_{13}(\sin^4\alpha + \cos^4\alpha) + (\bar{Q}_{11} + \bar{Q}_{33} - 4\bar{Q}_{55})\sin^2\alpha\cos^2\alpha,$$

$$K_{14} = \bar{Q}_{36}\cos^3\alpha + (\bar{Q}_{16} - 2\bar{Q}_{45})\sin^2\alpha\cos\alpha,$$

$$K_{15} = -(\bar{Q}_{13} - \bar{Q}_{33} + 2\bar{Q}_{55})\sin\alpha\cos^3\alpha - (\bar{Q}_{11} - \bar{Q}_{13} - 2\bar{Q}_{55})\sin^3\alpha\cos\alpha,$$

$$K_{16} = -\bar{Q}_{16}\sin^3\alpha - (\bar{Q}_{36} + 2\bar{Q}_{45})\sin\alpha\cos^2\alpha,$$

$$K_{22} = \bar{Q}_{22}, \quad K_{23} = \bar{Q}_{12}\cos^2\alpha + \bar{Q}_{23}\sin^2\alpha, \quad K_{24} = \bar{Q}_{26}\cos\alpha,$$

$$K_{25} = (\bar{Q}_{23} - \bar{Q}_{12})\sin\alpha\cos\alpha, \quad K_{26} = -\bar{Q}_{26}\sin\alpha,$$

$$K_{33} = \bar{Q}_{11}\cos^4\alpha + 2(\bar{Q}_{13} + 2\bar{Q}_{55})\sin^2\alpha\cos^2\alpha + \bar{Q}_{33}\sin^4\alpha,$$

$$K_{34} = \bar{Q}_{16}\cos^3\alpha + (\bar{Q}_{36} + 2\bar{Q}_{45})\sin^2\alpha\cos\alpha,$$

$$K_{35} = -(\bar{Q}_{13} - \bar{Q}_{33} + 2\bar{Q}_{55})\sin^3\alpha\cos\alpha - (\bar{Q}_{11} - \bar{Q}_{13} - 2\bar{Q}_{55})\sin\alpha\cos^3\alpha,$$

$$K_{36} = -\bar{Q}_{36}\sin^3\alpha - (\bar{Q}_{16} - 2\bar{Q}_{45})\sin\alpha\cos^2\alpha,$$

$$K_{44} = \bar{Q}_{44}\sin^2\alpha + \bar{Q}_{66}\cos^2\alpha,$$

$$K_{45} = -\bar{Q}_{45}\sin^3\alpha - (\bar{Q}_{16} - \bar{Q}_{36} - \bar{Q}_{45})\sin\alpha\cos^2\alpha,$$

$$K_{46} = (\bar{Q}_{44} - \bar{Q}_{66}) \sin\alpha \cos\alpha,$$

$$K_{55} = (\bar{Q}_{11} + \bar{Q}_{33} - 2\bar{Q}_{13} - 2\bar{Q}_{55}) \sin^2\alpha \cos^2\alpha + \bar{Q}_{55}(\sin^4\alpha + \cos^4\alpha),$$

$$K_{56} = \bar{Q}_{45} \cos^3\alpha + (\bar{Q}_{16} - \bar{Q}_{36} - \bar{Q}_{45}) \sin^2\alpha \cos\alpha,$$

$$K_{66} = \bar{Q}_{44} \cos^2\alpha + \bar{Q}_{66} \sin^2\alpha,$$

$$K_{ij} = K_{ji}, \quad i, j = 1, \ldots, 6,$$

where

$$\bar{Q}_{11} = C_{11} \cos^4\beta + 2(C_{12} + 2C_{66}) \sin^2\beta \cos^2\beta + C_{22} \sin^4\beta,$$

$$\bar{Q}_{12} = (C_{11} + C_{22} - 4C_{66}) \sin^2\beta \cos^2\beta + C_{12}(\sin^4\beta + \cos^4\beta),$$

$$\bar{Q}_{13} = C_{13} \cos^2\beta + C_{23} \sin^2\beta,$$

$$\bar{Q}_{16} = (C_{11} - C_{12} - 2C_{66}) \sin\beta \cos^3\beta + (C_{12} - C_{22} + 2C_{66}) \sin^3\beta \cos\beta,$$

$$\bar{Q}_{22} = C_{11} \sin^4\beta + 2(C_{12} + 2C_{66}) \sin^2\beta \cos^2\beta + C_{22} \cos^4\beta,$$

$$\bar{Q}_{23} = C_{13} \sin^2\beta + C_{23} \cos^2\beta,$$

$$\bar{Q}_{26} = (C_{11} - C_{12} - 2C_{66}) \sin^3\beta \cos\beta + (C_{12} - C_{22} + 2C_{66}) \sin\beta \cos^3\beta,$$

$$\bar{Q}_{33} = C_{33}, \quad \bar{Q}_{36} = (C_{13} - C_{23}) \sin\beta \cos\beta,$$

$$\bar{Q}_{44} = C_{44} \cos^2\beta + C_{55} \sin^2\beta,$$

$$\bar{Q}_{45} = (C_{55} - C_{44}) \sin\beta \cos\beta, \quad \bar{Q}_{55} = C_{44} \sin^2\beta + C_{55} \cos^2\beta,$$

$$\bar{Q}_{66} = (C_{11} + C_{22} - 2C_{12} - 2C_{66}) \sin^2\beta \cos^2\beta + C_{66}(\sin^4\beta + \cos^4\beta).$$

APPENDIX B: MATRIX COEFFICIENTS IN EQUATIONS (86)–(90)

Given here are the coefficients of the matrices in equations (86)–(90):

$$M_{Amn} \equiv \int_0^L m_o \xi_n \xi_m \, \mathrm{d}z + m_c \xi_n(z_c) \xi_m(z_c), \qquad M_{Bmn} \equiv \int_0^L I_o \alpha_n \alpha_m \, \mathrm{d}z + I_c \alpha_n(z_c) \alpha_m(z_c),$$

$$G_{Bmn} \equiv 2\Omega M_{Bnm}, \qquad K^s_{Amn} \equiv \int_0^L \kappa K^s_V \xi_n \xi'_m \, \mathrm{d}z, \qquad K^o_{Amn} \equiv \int_0^L \kappa K^o_V \xi'_n \xi'_m \, \mathrm{d}z,$$

$$K^s_{ABmn} \equiv \int_0^L (\kappa K^s_V \alpha_n \xi'_m + K^s_{VM} \alpha'_n \xi'_m) \, \mathrm{d}z, \qquad K^o_{ABmn} \equiv \int_0^L (\kappa K^o_V \alpha_n \xi'_m - K^o_{VM} \alpha'_n \xi'_m) \, \mathrm{d}z,$$

$$K^s_{BAmn} \equiv \int_0^L (\kappa K^s_{MV} \xi_n \alpha'_m + \kappa K^s_V \xi'_n \alpha_m) \, \mathrm{d}z, \qquad K^o_{BAmn} \equiv \int_0^L (-\kappa K^o_{MV} \xi_n \alpha'_m - \kappa K^o_V \xi'_n \alpha_m) \, \mathrm{d}z,$$

$$K^s_{Bmn} \equiv \int_0^L (K_M \alpha'_n \alpha'_m + \kappa K^s_{MV} \alpha_n \alpha'_m + K^s_{VM} \alpha'_n \alpha_m + \kappa K^s_V \alpha_n \alpha_m) \, \mathrm{d}z,$$

$$K^o_{Bmn} \equiv \int_0^L (-\kappa K^o_{MV}\alpha_n\alpha'_m + K^o_{VM}\alpha'_n\alpha_m - \kappa K^o_V\alpha_n\alpha_m)\,\mathrm{d}z,$$

$$M_{Cmn} \equiv \int_0^L m_o\eta_n\eta_m\,\mathrm{d}z + m_c\eta_n(z_c)\eta_m(z_c), \quad M_{Dmn} \equiv \int_0^L 2I_o\varphi_n\varphi_m\,\mathrm{d}z + 2I_c\varphi_n(z_c)\varphi_m(z_c),$$

$$K_{Cmn} \equiv \int_0^L K_P\eta'_n\eta'_m\,\mathrm{d}z, \qquad K_{CDmn} \equiv \int_0^L K_{PT}\varphi'_n\eta'_m\,\mathrm{d}z,$$

$$K_{DCmn} \equiv \int_0^L K_{TP}\eta'_n\varphi'_m\,\mathrm{d}z, \qquad K_{Dmn} \equiv \int_0^L K_T\varphi'_n\varphi'_m\,\mathrm{d}z.$$

For the numerical results presented, these coefficients are evaluated numerically using MAPLE.